nanomaterials

MDPI

Article

Efficient Blue to Red Afterglow Tuning in a Binary Nanocomposite Plastic Film

Yan Xia [1], Huase Ou [1], Wanbin Li [1], Gang Han [2] and Zhanjun Li [1,*]

[1] Guangdong Key Laboratory of Environmental Pollution and Health, School of Environment, Jinan University, Guangzhou 510632, China; yanxiajnu@sina.com (Y.X.); ouhuase@126.com (H.O.); gandeylin@126.com (W.L.)

[2] Department of Biochemistry and Molecular Pharmacology, University of Massachusetts Medical School, Worcester, MA 01605, USA; gang.han@umassmed.edu

* Correspondence: zjlisci@jnu.edu.cn

Received: 13 March 2018; Accepted: 16 April 2018; Published: 19 April 2018

Abstract: Colorful spectra are important for the diverse applications of persistent phosphors. A color conversion concept is developed to obtain abundant persistent luminescence color by mining capacities of known persistent phosphors with the most efficient persistent properties. Here, SiO_2/$Sr_2MgSi_2O_7$:Eu,Dy nanoparticles are chosen as a blue persistent luminescence donor nanophosphor, while ultrafine $CaAlSiN_3$:Eu is utilized as a red conversion phosphor to tune the persistent luminescence spectra from blue to red. The red afterglow emission can persist for more than 5 h. The decay of the red afterglow follows nearly the same kinetics as that of the blue one. Continuous color tuning can be successfully obtained by simply changing the mass ratio of the donor/conversion phosphor pair. This color conversion strategy may be significant in indicating numerous persistent/conversion nanocomposites or nanostructures and advance the development of persistent phosphors in diverse fields which need colorful spectral properties.

Keywords: persistent luminescence; afterglow; spectral tuning; nanophosphor; nanocomposite

1. Introduction

The emission of persistent phosphors can persist for a long period after excitation ceases. Persistent luminescence and persistent phosphors are arousing increasing interests and have found abundant applications in night vision materials, security signals, art painting, mechanical stress detection, high energy particle detection, optical information storage, catalysis, analysis, time-resolved bioimaging, etc. [1–3]. Apparently, these applications rely on the synthesis of persistent phosphors with abundant spectral properties. Many new phosphors have been reported, usually by developing new matrix and/or new dopants. For example, $Ca_{0.2}Mg_{0.9}Zn_{0.9}Si_2O_6$:Eu,Dy,Mn is the first studied persistent phosphor in persistent luminescence imaging [4,5]. Cr-doped gallium oxide related phosphors represent the current dominating ones [6–12]. Novel Cr/Ga-free persistent phosphors are being explored such as $Zn_3Ga_2Ge_2O_{10}$:Ni^{2+} [13], $LaAlO_3$:Mn^{4+},Ge^{4+} [14], $BaZrSi_3O_9$: Eu^{2+}, Pr^{3+} [15], $KGaGeO_4$:Bi^{3+} [16], semiconducting polymer [17], metal organic framework [18]. To date, $Sr_2MgSi_2O_7$:Eu^{2+},Dy^{3+} still represents one of the most efficient commercial ones [19,20]. However, there is still not a red persistent phosphor with afterglow properties close to the commercialized blue or green ones. A novel strategy is needed to realize efficient red persistent luminescence to facilitate the practical applications of persistent phosphors.

Color conversion has been widely applied in the field of LED lighting to obtain white light [21]. Generally, a blue semiconductor lighting chip and color conversion phosphors are mixed together. Then, the color conversion phosphors absorb part of the blue light and emit green, yellow, and/or

red light to generate abundant visible colors [22–25]. Yuhua Wang's group successfully introduced color conversion to generate white persistent luminescence by using $CaAl_2O_4$:Eu^{2+},Nd^{3+} bulk material as blue persistent phosphor and $Y_3Al_5O_{12}$:Ce^{3+} as conversion phosphor [26]. As bulk raw materials were used, the amount of conversion phosphor has to be as much as 50% which will decrease the emission intensity and lead to heterogeneity. Using nanophosphors may generate more efficient color conversion or energy transfer. Inspired by these previous works, we propose that persistent spectral tuning can be realized efficiently by exploring known persistent nanophosphors via color conversion. Here, a blue persistent nanophosphor, SiO_2/$Sr_2MgSi_2O_7$:Eu^{2+},Dy^{3+} nanoparticle (SMS), is chosen as a blue persistent energy donor as $Sr_2MgSi_2O_7$:Eu^{2+},Dy^{3+} is currently one of the most efficient blue persistent phosphors [27,28] and can be easily synthesized in nanoscale [19–29]. $CaAlSiN_3$:Eu^{2+} (CASN), which is one of the most efficient red color conversion phosphors in LED industry, is used as a color conversion phosphor [30–32]. SMS and CASN ultrafine particles are used to obtain a uniform binary persistent luminescence nanocomposite system. The nanocomposite is buried into polymethyl methacrylate (PMMA) plastic film to make the particles stay close to each other and thus to ensure efficient conversion efficiency.

2. Experimental

2.1. Synthesis of SMS

The synthesis of SMS was according to our reported template method with modifications [33,34]. Briefly, 0.1273 mol of $Mg(NO_3)_2{\cdot}6H_2O$, 0.0667 mol of $Sr(NO_3)_2$, 0.01 mol of HBO_3, 0.002 mol of $Eu(NO_3)_3$, and 0.004 mol of $Dy(NO_3)_3$ were dissolved in deionized water with a total volume of 100 mL according to the formula of $Sr_2MgSi_2O_7$:$Eu_{0.01}$,$Dy_{0.02}$, forming a precursor solution of SMS. The total molar concentration of metal ions was controlled to be 2 M. Five percent (molar ratio vs. metal ions) of HBO_3 was used as flux. Ten grams of mesoporous silica nanoparticles (100 nm–150 nm) were mixed with 100 mL of SMS precursor solution, stirred for 1 h, centrifuged, and dried at 105 °C for 2 h. The dried precursor was firstly annealed at 800 °C for 2 h. The product was ground using a motor and pestle. SMS nanoparticles were finally obtained after being annealed at 1000 °C for 5 min at a heating rate of 10 °C/min. Both of the heating procedures were carried out at a reductive (H_2/Ar, 10%) atmosphere.

2.2. Synthesis of CASN

CASN was prepared by a reported solid state method followed by a ball milling process [31].

2.3. SMS/CASN Film Preparation

SMS/CASN composite with diverse mass ratio was homogenized by ball milling. Then, 0.1 g of the composite was mixed with 1 mL of PMMA/dichloroform (20%) solution. The mass content of PMMA in the film is ca. 66.7 wt %. The mixture was stirred at room temperature to let dichloroform evaporate and form a slurry, which was poured into a round mould with a diameter of ~2 cm and a thickness of 1 mm. A SMS/CASN plastic film was obtained after aging the mould in open air at room temperature (~20 °C) overnight.

2.4. Characterization

The X-ray diffraction pattern was acquired by using a powder diffractometer with Cu Kα radiation (λ = 1.5418 Å) (D2 PHASER, AXS, Karlsruhe, Germany). The photoluminescence and persistent luminescence spectra were obtained by using a fluorophotometer (Lumina, ThermoFisher, Waltham, MA, USA). The afterglow spectra were activated by using a violet LED torch (395 nm, 9 w) and acquired at 10 min after the stop of excitation. The microstructures of the phosphors were observed by using a field emission scanning electron microscope with an accelerating voltage of 5 kV (S-4800, Hitachi,

Tokyo, Japan). Three-dimensional luminescent imaging of the nanocomposite film samples was conducted using a Bio-Rad gel imaging system.

3. Results and Discussion

Alkaline earth silicate nanoparticles can be synthesized by using mesoporous silica nanoparticles as morphology-controlling templates, forming a nanocomposite of quartz and persistent phosphors [33,34]. As indicated in Figure 1a, the diffraction pattern of the as-synthesized SMS corresponds well with that of tetragonal $Sr_2MgSi_2O_7$ (JCPDS card no. 01-075-1736) and hexaganol SiO_2 (JCPDS card no. 01-086-1629). No apparent impurity diffraction peaks can be observed, indicating the successful doping of Eu and Dy into $Sr_2MgSi_2O_7$ lattice. The size of SMS particles ranges from ~80 nm to ~150 nm. The as-synthesized CASN possesses an orthorhombic crystal structure with diffraction pattern corresponding with JCPDS card no. 00-039-0747 (Figure 1b). The as-synthesized CASN has a size ranging from ~200 nm to ~2 μm. Both SMS and CASN samples have relatively small sizes which is smaller than most of the commercial LED conversion phosphors (~10 μm). Thus, uniform homogenization and efficient color conversion may be possible.

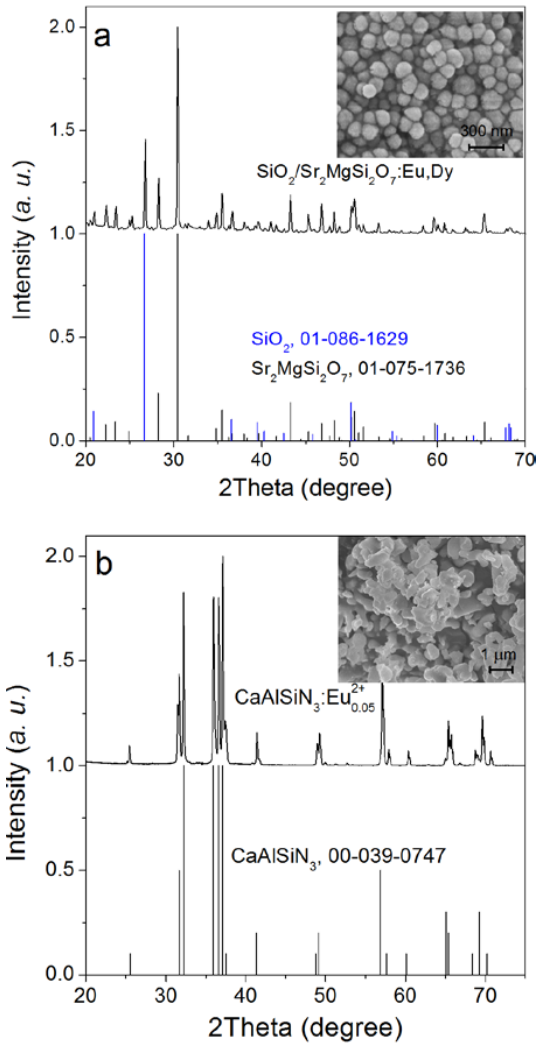

Figure 1. X-ray diffraction patterns and scanning electron microscopy images of the as-synthesized SMS ($SiO_2/Sr_2MgSi_2O_7:Eu^{2+},Dy^{3+}$ nanoparticle) (**a**) and CASN ($CaAlSiN_3:Eu^{2+}$) (**b**) ultrafine particles.

In order to establish an efficient color conversion luminescence system, an overlap between the donor/acceptor is a prerequisite [35–37]. The photoluminescence excitation/emission spectra of CASN in Figure 2 indicate that CASN phosphor can be efficiently excited by wide spectrum extended from UV to 600 nm and emit red light peaking at ~660 nm. Notably, its excitation spectrum overlays well with the persistent luminescence spectrum of SMS from 430 nm to 550 nm with a peak at ~470 nm. Thus, CASN can serve as a possible efficient conversion phosphor for SMS. We prepared a nanocomposite of SMS and CASN which contains 20% (by weight) of CASN mixed by ball milling and then buried into PMMA film. After excited by a blue LED torch, the as-prepared SMS/CASN/PMMA film possessed bright red afterglow persistent luminescence in the dark. Its afterglow emission spectrum possessed a weak blue peak at ~470 nm and an intense red one at ~660 nm (Figure 3). The blue peak comes from the typical afterglow emission of Eu^{2+} in SMS. The red peak comes from the photoluminescence of Eu^{2+} in CASN. The high red/blue ratio indicates a successful color conversion process.

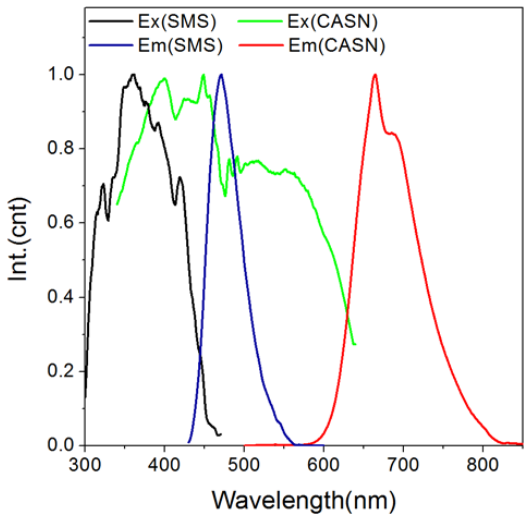

Figure 2. Photoluminescence excitation/emission spectra of the as-synthesized SMS and CASN nanoparticles, respectively. The excitation spectra of SMS and CASN were monitored at 470 nm and 665 nm, respectively. The emission spectra of SMS and CASN were excited at 400 nm and 470 nm, respectively.

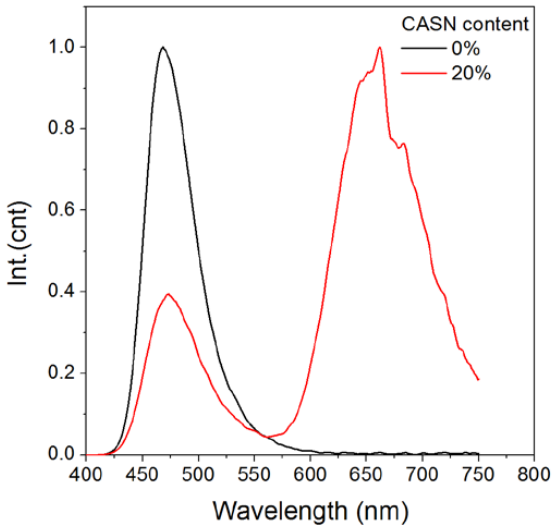

Figure 3. Afterglow emission of SMS and CASN/SMS nanocomposite PMMA (polymethyl methacrylate) film (20% of CASN by weight). Samples are excited by using a violet LED torch (395 nm, 9 w).

The afterglow emission of the CASN/SMS nanocomposite PMMA film can be detected for more than 5 h at 470 nm/660 nm, as shown in Figure 4a. Its decay kinetics can be fitted successfully by a ExpDec2 function, $y = A_1 \cdot \exp(-x/t_1) + A_2 \cdot \exp(-x/t_2) + y_0$, using origin software, as shown in Table 1. The similar values of t_1 and t_2 in the fitted decay curves of 470 nm and 660 nm indicate that the afterglow emissions at 470 nm and 660 nm follow similar decay kinetics and can ensure stable color during its decay process. The afterglow intensity ratio of Int.(660 nm) vs. Int.(470 nm) fluctuates at a narrow range from 2.5 to 2.7 within 5 h during the whole afterglow process, which also indicates stable spectral color of the afterglow emission. Both of the two decay curves include a fast decay period and a relatively slow one. The fast decay period in the beginning comes from the release of the stored energy in shallow traps, while the slow one originates from the release of the stored energy in deeper energy traps. Similar results have been revealed in previous reports about afterglow mechanisms of $Sr_2MgSi_2O_7$:Eu,Dy [38–40].

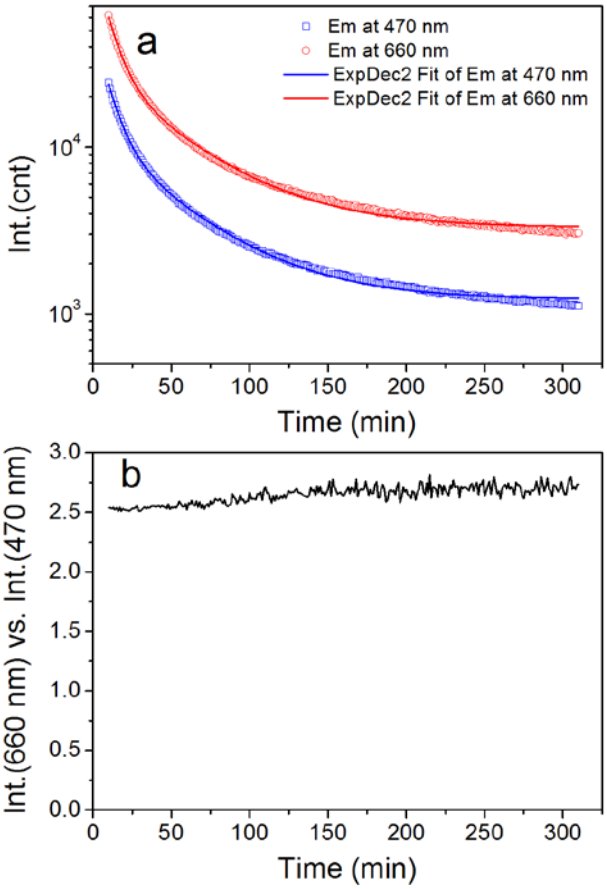

Figure 4. Afterglow decay of the CASN/SMS (1/4, by weight) nanocomposite film: (**a**) Emission at 470 nm/660 nm; (**b**) red/blue intensity ratio, Int.(660 nm/Int.(470 nm), within 300 min. A 10 min delay was used because of the intense luminescence intensity at the start of the decay process and the over range protection of the fluorophotometer.

Table 1. Decay kinetic parameters of the afterglow emission of CASN/SMS (CASN content, 20 wt %) nanocomposite.

Wavelength/nm	t_1/min	t_2/min	A_1	A_2	R^2
470	8.8	48.1	42,980	10,797	0.9994
660	8.9	48.8	111,110	26,721	0.9993

In order to study the influence of mass ratio to spectral tuning, CASN/SMS nanocomposite films with diverse mass ratios were prepared. Their afterglow emission spectra (Figure 5) show the blue persistent luminescence of SMS at ~470 nm. A new peak appears at ~660 nm, which can be assigned to the fluorescence emission of CASN excited by the persistent luminescence of SMS. As indicated in Figure 6, the blue peak decreases because of the decrease of the mass of SMS in the film and the absorption of CASN along with the increasing amount of CASN in the film. Higher red/blue ratio (Int.(660 nm) vs. Int.(470 nm)), which means redder visual color, can be obtained if more CASN is used. Yet, the total persistent luminescence intensity will decrease along with an increasing CASN content due to less SMS exists. The optimal mass ratio of CASN vs. (CASN + SMS) is found to be 10% because of its maximal emission at 660 nm in all the film samples which has a red/blue ratio of ~1.2. Notably, a relatively small amount of conversion phosphor (~10%) is needed to generate a successful and apparent persistent luminescence color conversion process, possibly because of the ultrafine particle sizes of SMS and CASN which provides uniform homogenization. Regarding energy transfer between particles, a small distance is generally favorable. Using SMS nanoparticles may possibly limit the distance between the persistent luminescence energy donor and conversion phosphor within the range of ca. 100 nm and realize more efficient persistent luminescence color conversion. According to a recent publication, 50% or more conversion phosphors will be needed to realize apparent color conversion in the case of bulk phosphors [26]. Thus, nanocomposites or nanostructures may be a possible efficient new way to explore abundant persistent luminescence spectra by taking full advantage of existing persistent phosphors and conversion phosphors.

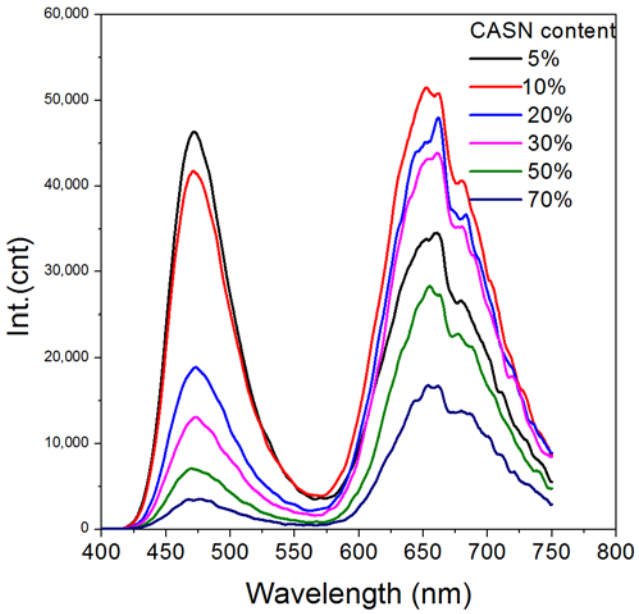

Figure 5. Afterglow emission spectra of CASN/SMS nanocomposite films with diverse CASN content. Samples are excited by using a violet LED torch (395 nm, 9 w).

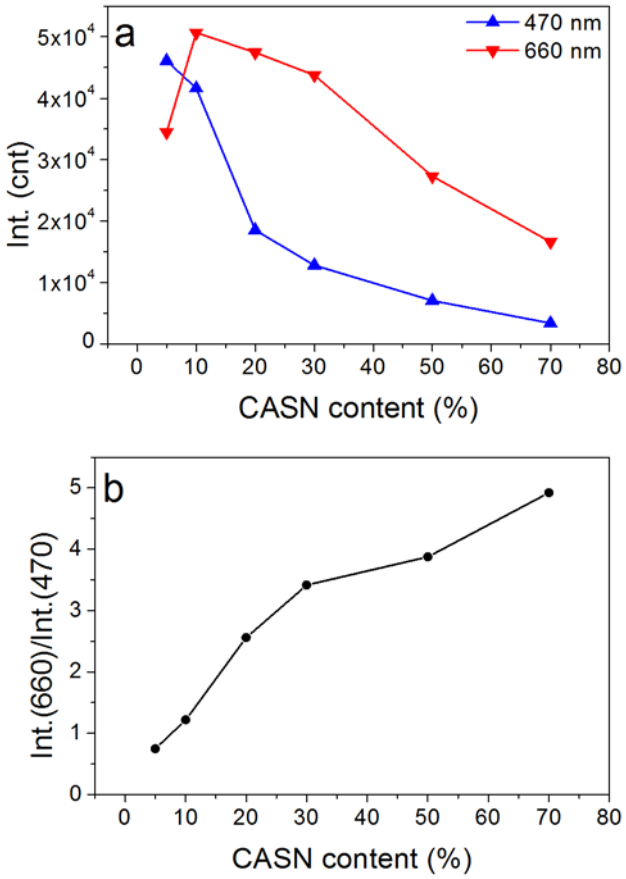

Figure 6. Influence of CASN content on the intensity (**a**) and red/blue emission ratios (**b**) (Int.(660 nm) vs. Int.(470 nm)) of the nanocomposite films.

The visible color of the samples can be gradually tuned from blue (SMS) to deep red when the content of CASN is increased from 0% to 70% (Figure 7). Regarding to red persistent luminescence, $Y_2O_2S:Eu^{3+},Mg^{2+},Ti^{4+}$ and $CaS:Eu^{2+},Tm^{3+}$ are representative commercial persistent phosphors. However, $Y_2O_2S:Eu^{3+},Mg^{2+},Ti^{4+}$ can only be excited efficiently by UV or violet light because of the spin-forbidden 4*f*-4*f* transition of Eu^{3+}, which means that it can't be excited efficiently by room light, which will hinder its practical applications [41]. $CaS:Eu^{2+},Tm^{3+}$ can be excited efficiently by room light but suffers from fast decay and poor water resistance [42]. SMS/CASN composite film possesses bright red persistent luminescence after blue light excitation, which can be seen for more than 5 h in the dark by naked eyes. 3-D luminescence imaging was performed in a bio-rad gel imaging system to study the luminescence homogeneity of the composite films, in which the intensity of each pixel is expressed in false rainbow color (blue to red colors represent intensities from weak to strong) and height. The result in Figure 7B indicates that the use of nanoscale or ultrafine particles can provide good spatial color homogeneity. The multicolor afterglow nanocomposite may be painted into colorful afterglow patterns like afterglow logo and bar code as shown in Figure 7C. Thus, this color conversion strategy may find potential applications such as anti-fake painting, information encryption, safety identification, and in energy saving lighting strategies.

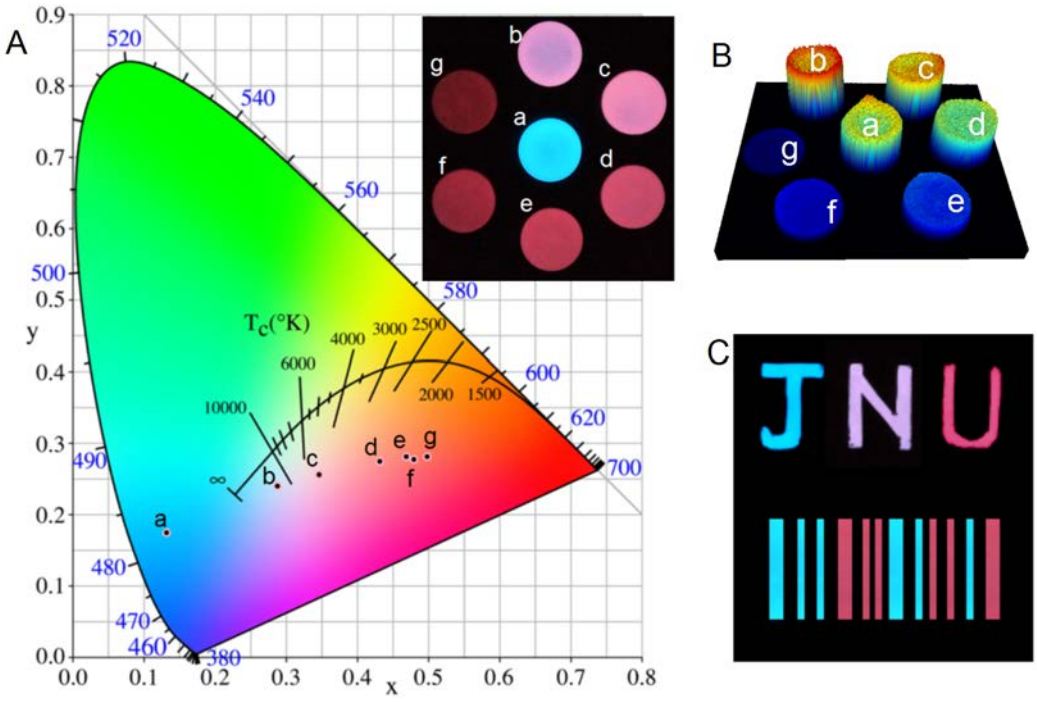

Figure 7. (**A**) CIE (Commission Internationale de L'Eclairage) chromaticity diagram and digital pictures of the multicolor SMS/CASN nanocomposite film samples with diverse CASN contents. (**a**) 0%, (**b**) 5%, (**c**) 10%, (**d**) 20%, (**e**) 30%, (**f**) 50%, and (**g**) 70%. The digital pictures were taken by using a SLR (single-lens reflex) camera after the stop of LED excitation (395 nm) for 5 min; (**B**) Three-dimensional luminescent imaging of the nanocomposite film samples (diameter 2 cm, thickness ~0.2 mm). The luminescence intensity is expressed by false color and height; (**C**) Potential applications of multicolor afterglow nanocomposite. The letters J, N, and U are painted by using nanocomposites with CASN contents of 0%, 5%, and 20%, respectively. The bar code is painted by using nanocomposites with CASN contents of 0% (blue) and 20% (red).

4. Conclusions

SMS, an efficient blue persistent nanophosphor, can serve as an efficient persistent nanometer energy donor to excite CASN, a red emitting phosphor without persistent properties. The red afterglow emission can persist for more than 5 h. The decay of the red afterglow follows nearly the same kinetics as that of the blue one. The continuous color tuning afterglow nanocomposite material or device can be obtained by simply changing the mass ratio of the donor persistent nanophosphor and conversion phosphor. Although this work only extends the persistent luminescence spectra from blue to deep red, we believe that near infrared persistent luminescence may also be realized by using a similar strategy. In addition, this work may be significant in indicating possible efficient persistent luminescence nanostructures and nanodevices in the future. This work may further advance the development of colorful persistent phosphors in diverse fields.

Acknowledgments: This research was supported by the National Natural Science Foundation of China (21701052), the National Natural Science Foundation of Guangdong Province of China (32217073), the Special Funds for Basic Scientific Research Operations of Central Universities of China (11617323).

Author Contributions: Y.X. and H.O. conceived and designed the experiments; Y.X. and Z.L. performed the experiments; Y.X., W.L., and Z.L. analyzed the data; Y.X. wrote the paper; Z.L. and G.H. revised the paper; Z.L. supervised the research project.

Conflicts of Interest: The authors declare no conflict of interest.

References

1. Lecuyer, T.; Teston, E.; Ramirez-Garcia, G.; Maldiney, T.; Viana, B.; Seguin, J.; Mignet, N.; Scherman, D.; Richard, C. Chemically engineered persistent luminescence nanoprobes for bioimaging. *Theranostics* **2016**, *6*, 2488–2524. [CrossRef] [PubMed]
2. Li, Y.; Gecevicius, M.; Qiu, J.R. Long persistent phosphors-from fundamentals to applications. *Chem. Soc. Rev.* **2016**, *45*, 2090–2136. [CrossRef] [PubMed]
3. Wang, J.; Ma, Q.; Wang, Y.; Shen, H.; Yuan, Q. Recent progress in biomedical applications of persistent luminescence nanoparticles. *Nanoscale* **2017**, *9*, 6204–6218. [CrossRef] [PubMed]
4. Chermont, Q.L.; Chaneac, C.; Seguin, J.; Pelle, F.; Maitrejean, S.; Jolivet, J.P.; Gourier, D.; Bessodes, M.; Scherman, D. Nanoprobes with near-infrared persistent luminescence for in vivo imaging. *Proc. Natl. Acad. Sci. USA* **2007**, *104*, 9266–9271. [CrossRef] [PubMed]
5. Zhang, L.; Lei, J.; Liu, J.; Ma, F.; Ju, H. Persistent luminescence nanoprobe for biosensing and lifetime imaging of cell apoptosis via time-resolved fluorescence resonance energy transfer. *Biomaterials* **2015**, *67*, 323–334. [CrossRef] [PubMed]
6. Pan, Z.W.; Lu, Y.Y.; Liu, F. Sunlight-activated long-persistent luminescence in the near-infrared from Cr^{3+}-doped zinc gallogermanates. *Nat. Mater.* **2012**, *11*, 58–63. [CrossRef] [PubMed]
7. Maldiney, T.; Bessiere, A.; Seguin, J.; Teston, E.; Sharma, S.K.; Viana, B.; Bos, A.J.J.; Dorenbos, P.; Bessodes, M.; Gourier, D.; et al. The in vivo activation of persistent nanophosphors for optical imaging of vascularization, tumours and grafted cells. *Nat. Mater.* **2014**, *13*, 418–426. [CrossRef] [PubMed]
8. Li, Z.J.; Zhang, Y.W.; Wu, X.; Huang, L.; Li, D.S.; Fan, W.; Han, G. Direct Aqueous-Phase Synthesis of Sub-10 nm "Luminous Pearls" with Enhanced in Vivo Renewable Near-Infrared Persistent Luminescence. *J. Am. Chem. Soc.* **2015**, *137*, 5304–5307. [CrossRef] [PubMed]
9. Shi, J.P.; Sun, M.; Sun, X.; Zhang, H.W. Near-infrared persistent luminescence hollow mesoporous nanospheres for drug delivery and in vivo renewable imaging. *J. Mater. Chem. B* **2016**, *4*, 7845–7851. [CrossRef]
10. Chen, L.J.; Yang, C.X.; Yan, X.P. Liposome-Coated Persistent Luminescence Nanoparticles as Luminescence Trackable Drug Carrier for Chemotherapy. *Anal. Chem.* **2017**, *89*, 6936–6939. [CrossRef] [PubMed]
11. Xue, Z.; Li, X.; Li, Y.; Jiang, M.; Liu, H.; Zeng, S.; Hao, J. X-ray-Activated Near-Infrared Persistent Luminescent Probe for Deep-Tissue and Renewable in Vivo Bioimaging. *ACS Appl. Mater. Interfaces* **2017**, *9*, 22132–22142. [CrossRef] [PubMed]
12. Ueda, J.; Kuroishi, K.; Tanabe, S. Bright persistent ceramic phosphors of Ce^{3+}-Cr^{3+}-codoped garnet able to store by blue light. *Appl. Phys. Lett.* **2014**, *104*, 101904. [CrossRef]
13. Liu, F.; Liang, Y.J.; Chen, Y.F.; Pan, Z.W. Divalent Nickel-Activated Gallate-Based Persistent Phosphors in the Short-Wave Infrared. *Adv. Opt. Mater.* **2016**, *4*, 562–566. [CrossRef]
14. Li, Y.; Li, Y.Y.; Sharafudeen, K.; Dong, G.P.; Zhou, S.F.; Ma, Z.J.; Peng, M.Y.; Qiu, J.R. A strategy for developing near infrared long-persistent phosphors: Taking $MAlO_3$:Mn^{4+},Ge^{4+} (M = La, Gd) as an example. *J. Mater. Chem. C* **2014**, *2*, 2019–2027. [CrossRef]
15. Guo, H.J.; Wang, Y.H.; Li, G.; Liu, J.; Feng, P.; Liu, D.W. Cyan emissive super-persistent luminescence and thermoluminescence in $BaZrSi_3O_9$: Eu^{2+}, Pr^{3+} phosphors. *J. Mater. Chem. C* **2017**, *5*, 2844–2851. [CrossRef]
16. Sun, W.Z.; Pang, R.; Li, H.M.; Li, D.; Jiang, L.H.; Zhang, S.; Fu, J.P.; Li, C.Y. Investigation of a novel color tunable long afterglow phosphor $KGaGeO_4$:Bi^{3+}: Luminescence properties and mechanism. *J. Mater. Chem. C* **2017**, *5*, 1346–1355. [CrossRef]
17. Palner, M.; Pu, K.Y.; Shao, S.; Rao, J.H. Semiconducting Polymer Nanoparticles with Persistent Near-Infrared Luminescence for In Vivo Optical Imaging. *Angew. Chem. Int. Ed.* **2015**, *54*, 11477–11480. [CrossRef] [PubMed]
18. Yang, X.G.; Yan, D.P. Long-afterglow metal-organic frameworks: Reversible guest-induced phosphorescence tunability. *Chem. Sci.* **2016**, *7*, 4519–4526. [CrossRef]
19. Van den Eeckhout, K.; Smet, P.F.; Poelman, D. Persistent Luminescence in Eu^{2+}-Doped Compounds: A Review. *Materials* **2010**, *3*, 2536–2566. [CrossRef]
20. Zhuang, Y.X.; Katayama, Y.; Ueda, J.; Tanabe, S. A brief review on red to near-infrared persistent luminescence in transition-metal-activated phosphors. *Opt. Mater.* **2014**, *36*, 1907–1912. [CrossRef]
21. Smet, P.F.; Parmentier, A.B.; Poelman, D. Selecting Conversion Phosphors for White Light-Emitting Diodes. *J. Electrochem. Soc.* **2011**, *158*, R37–R54. [CrossRef]

22. Palazon, F.; Di Stasio, F.; Akkerman, Q.A.; Krahne, R.; Prato, M.; Manna, L. Polymer-Free Films of Inorganic Halide Perovskite Nanocrystals as UV-to-White Color-Conversion Layers in LEDs. *Chem. Mater.* **2016**, *28*, 2902–2906. [CrossRef] [PubMed]
23. Pust, P.; Weiler, V.; Hecht, C.; Tucks, A.; Wochnik, A.S.; Henss, A.K.; Wiechert, D.; Scheu, C.; Schmidt, P.J.; Schnick, W. Narrow-band red-emitting $Sr[LiAl_3N_4]:Eu^{2+}$ as a next-generation LED-phosphor material. *Nat. Mater.* **2014**, *13*, 891–896. [CrossRef] [PubMed]
24. Huang, H.; Chen, B.K.; Wang, Z.G.; Hung, T.F.; Susha, A.S.; Zhong, H.Z.; Rogach, A.L. Water resistant $CsPbX_3$ nanocrystals coated with polyhedral oligomeric silsesquioxane and their use as solid state luminophores in all-perovskite white light-emitting devices. *Chem. Sci.* **2016**, *7*, 5699–5703. [CrossRef]
25. Oh, J.H.; Kang, H.; Eo, Y.J.; Park, H.K.; Do, Y.R. Synthesis of narrow-band red-emitting $K_2SiF_6:Mn^{4+}$ phosphors for a deep red monochromatic LED and ultrahigh color quality warm-white LEDs. *J. Mater. Chem. C* **2015**, *3*, 607–615. [CrossRef]
26. Chen, W.B.; Wang, Y.H.; Zeng, W.; Han, S.C.; Li, G.; Guo, H.J.; Li, Y.Y.; Qiang, Q.P. Long persistent composite phosphor $CaAl_2O_4:Eu^{2+},Nd^{3+}/Y_3Al_5O_{12}:Ce^{3+}$: A novel strategy to tune the colors of persistent luminescence. *New J. Chem.* **2016**, *40*, 485–491. [CrossRef]
27. Pan, W.; Ning, G.L.; Zhang, X.; Wang, J.; Lin, Y.; Ye, J.W. Enhanced luminescent properties of long-persistent $Sr_2MgSi_2O_7:Eu^{2+}$, Dy^{3+} phosphor prepared by the co-precipitation method. *J. Lumin.* **2008**, *128*, 1975–1979. [CrossRef]
28. Shi, X.D.; Sho, L.; Li, M.Z.; Hou, J.; Chen, L.F.; Ye, C.Q.; Shen, W.Z.; Jiang, L.; Song, Y.L. Efficient Luminescence of Long Persistent Phosphor Combined with Photonic Crystal. *ACS Appl. Mater. Interfaces* **2014**, *6*, 6317–6321. [CrossRef] [PubMed]
29. Homayoni, H.; Ma, L.; Zhang, J.Y.; Sahi, S.K.; Rashidi, L.H.; Bui, B.; Chen, W. Synthesis and conjugation of $Sr_2MgSi_2O_7:Eu^{2+}$, Dy^{3+} water soluble afterglow nanoparticles for photodynamic activation. *Photodiagn. Photodyn. Ther.* **2016**, *16*, 90–99. [CrossRef] [PubMed]
30. Lee, S.; Sohn, K.S. Effect of inhomogeneous broadening on time-resolved photoluminescence in $CaAlSiN_3:Eu^{2+}$. *Opt. Lett.* **2010**, *35*, 1004–1006. [CrossRef] [PubMed]
31. Lei, B.; Machida, K.; Horikawa, T.; Hanzawa, H. Synthesis and Photoluminescence Properties of $CaAlSiN_3:Eu^{2+}$ Nanocrystals. *Chem. Lett.* **2010**, *39*, 104–105. [CrossRef]
32. Piao, X.; Machida, K.; Horikawa, T.; Hanzawa, H.; Shimomura, Y.; Kijima, N. Preparation of $CaAlSiN_3:Eu^{2+}$ Phosphors by the Self-Propagating High-Temperature Synthesis and Their Luminescent Properties. *Chem. Mater.* **2007**, *19*, 4592–4599. [CrossRef]
33. Li, Z.J.; Zhang, H.W.; Sung, M.; Shen, J.S.; Fu, H.X. A facile and effective method to prepare long-persistent phosphorescent nanospheres and its potential application for in vivo imaging. *J. Mater. Chem.* **2012**, *22*, 24713–24720.
34. Li, Z.; Shi, J.; Zhang, H.; Sun, M. Highly controllable synthesis of near-infrared persistent luminescence $SiO_2/CaMgSi_2O_6$ composite nanospheres for imaging in vivo. *Opt. Express* **2014**, *22*, 10509–10518. [CrossRef] [PubMed]
35. Xia, Z.G.; Liu, Q.L. Progress in discovery and structural design of color conversion phosphors for LEDs. *Prog. Mater. Sci.* **2016**, *84*, 59–117. [CrossRef]
36. Fresta, E.; Costa, R.D. Beyond traditional light-emitting electrochemical cells—A review of new device designs and emitters. *J. Mater. Chem. C* **2017**, *5*, 5643–5675. [CrossRef]
37. Qin, X.; Liu, X.W.; Huang, W.; Bettinelli, M.; Liu, X.G. Lanthanide-Activated Phosphors Based on 4f-5d Optical Transitions: Theoretical and Experimental Aspects. *Chem. Rev.* **2017**, *117*, 4488–4527. [CrossRef] [PubMed]
38. Lin, Y.H.; Tang, Z.L.; Zhang, Z.T.; Wang, X.X.; Zhang, J.Y. Preparation of a new long afterglow blue-emitting $Sr_2MgSi_2O_7$-based photoluminescent phosphor. *J. Mater. Sci. Lett.* **2001**, *20*, 1505–1506. [CrossRef]
39. Fei, Q.; Chang, C.K.; Mao, D.L. Luminescent properties of $Sr_2MgSi_2O_7$ and $Ca_2MgSi_2O_7$ long lasting phosphors activated by Eu^{2+}, Dy^{3+}. *J. Alloy Compd.* **2005**, *390*, 133–137. [CrossRef]
40. Lin, Y.H.; Nan, C.W.; Zhou, X.S.; Wu, J.B.; Wang, H.F.; Chen, D.P.; Xu, S.M. Preparation and characterization of long afterglow $M_2MgSi_2O_7$-based (M: Ca, Sr, Ba) photoluminescent phosphors. *Mater. Chem. Phys.* **2003**, *82*, 860–863. [CrossRef]

41. Li, W.; Liu, Y.; Ai, P.; Chen, X. Synthesis and characterization of $Y_2O_2S:Eu^{3+}$, Mg^{2+}, Ti^{4+} nanorods via a solvothermal routine. *J. Rare Earth* **2009**, *27*, 895–899. [CrossRef]
42. Jia, D. Enhancement of long-persistence by CeCo-doping in $CaS:Eu^{2+}$, Tm^{3+} red phosphor. *J. Electrochem. Soc.* **2006**, *153*, H198–H201. [CrossRef]